Journal of Hazardous Materials 390 (2020) 122136

Contents lists available at ScienceDirect

Journal of Hazardous Materials

journal homepage: www.elsevier.com/locate/jhazmat

Mineralogical evidence of unfavorable geochemical interactions between urban runoff pollutants and filter materials in low-impact systems

Marcelino Antonio Zúñiga-Estrada[a], Gabriela A. Vázquez-Rodríguez[a], Màrius Ramírez-Cardona[b], Liliana Lizárraga-Mendiola[c,*]

[a] Área Académica de Química, Universidad Autónoma del Estado de Hidalgo, Km. 4.5, Carr. Pachuca-Tulancingo, 42086, Mineral de la Reforma, Hidalgo, Mexico
[b] Área Académica de Ciencias de la Tierra y Materiales (address as[a]), Mexico
[c] Área Académica de Ingeniería y Arquitectura (address as[a]), Mexico

GRAPHICAL ABSTRACT

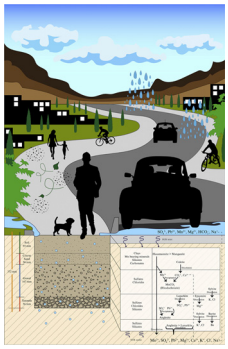

ARTICLE INFO

Editor: Daniel C.W. Tsang

Keywords:
Urban runoff
Heavy metals
Bioretention
Low-impact development
Infiltration

ABSTRACT

We report on the geochemical interactions between a synthetic urban runoff (SUR) and the minerals of materials used in a multi-layered column filter (soil, sand, gravel, and tezontle) at the laboratory scale, which mimicked an unvegetated low-impact development (LID) system. After five 8 h infiltration cycles using the SUR, the average concentrations of Pb and Mn decreased slightly at the column outlet, as did HCO_3^-, SO_4^{2-}, and Na^+, whereas Mg increased and Cl^-, Ca^{2+}, and K^+ were only detected at the outlet. The filter materials were comprised of silicates, Mn-bearing oxides (hausmannite and manganite), carbonates (calcite), chlorides (sylvite), and sulfates (anglesite, lanarkite, barite, and epsomite). PHREEQC modeling allowed the identification of the geochemical processes that occurred in the filter. The results showed the removal capacity of the filter materials through the formation of secondary minerals such as rhodochrosite ($MnCO_3$) and the over-saturation of anglesite ($PbSO_4$), and also showed that they may mobilize ions from the upper to the interior layers (as Mg^{2+} from epsomite, $MgSO_4{\cdot}7H_2O$, and Ba^{2+} from barite, $BaSO_4$). We highlight the importance of knowing the geological nature of filter materials used in LID systems because they may lead to the geogenic mobilization of toxic contaminants to the environment.

* Corresponding author.
E-mail addresses: lililga.lm@gmail.com, mendiola@uaeh.edu.mx (L. Lizárraga-Mendiola).

https://doi.org/10.1016/j.jhazmat.2020.122136
Received 12 September 2019; Received in revised form 15 January 2020; Accepted 17 January 2020
Available online 18 January 2020

1. Introduction

The growth of urban areas leads to the waterproofing of surfaces that previously facilitated the infiltration of surface runoff and the natural recharge of aquifers. To overcome this problem, low-impact development (LID) systems are receiving attention for the recovery of perviousness in built environments. Bioretention cells, vegetated swales, and infiltration trenches, among others, are LID systems that are extensively used because they are easily adapted to urban areas. These systems are installed where the site hydrology favors the infiltration of urban surface runoff, while maintaining a minimal negative impact on infrastructure. The benefits of LID include low maintenance requirements, high volumes of surface runoff captured (Goulden et al., 2018), and the mitigation of flooding risks (Nguyen et al., 2019). The traditional goals of LID systems have been aquifer recharge and urban runoff reclamation for non-potable purposes; however, they are increasingly being used as valuable water pollution prevention tools (Ortega-Villar et al., 2019).

LID systems rely on the use of natural materials (i.e., soil, gravel, and sand; Song et al., 2015; Monrabal-Martínez et al., 2018), in which pollutants within runoff are intercepted, adsorbed, and stored or transformed. Coarse soils such as loamy sands, loams, or sandy loams are normally used to enhance infiltration (Monrabal-Martínez et al., 2018). LID technologies such bioretention cells, rain gardens, or vegetated swales also use plants to restore the landscape ability to manage water, and to exploit their unique phytoremediation mechanisms. Some studies have focused on the capacity of LID systems to improve water quality (Ivanovsky et al., 2018). Others have focused on elucidating the removal mechanisms involved in order to determine the efficiency of LID systems, mainly towards heavy metals (Kabir et al., 2017; Walaszek et al., 2018), although their efficiency for nutrient removal has also been studied (Wang et al., 2017; Robertson et al., 2018). In addition, some studies have been conducted to enhance the pollutant adsorption capacity of LID systems by adding engineered materials, such as Fe and Al oxide granules to enhance sorption capacity (Shrestha et al., 2018). Recently, biochar (a carbonaceous adsorbent made through pyrolysis of organic waste) has been proposed as a high-performance material that enhances the decontamination potential of LID systems (Lau et al., 2017). Besides, biochar increases water storage and mitigate plant drought stress in vegetated LID devices (Mohanty et al., 2018; Sun et al., 2020). Engineered filter media must also maintain a high hydraulic conductivity, and consequently coarse-grained materials are preferred.

Managed aquifer recharge studies have demonstrated that several physicochemical processes can occur between groundwater and bedrock minerals, thus leading to deleterious effects on water quality (Vanderzalm et al., 2010). For instance, Fe and Mn may be incorporated into water through the dissolution of mineral oxides, and As can be mobilized from bedrock following the oxidation of pyrite (Page et al., 2018). Changes in the mineralogical composition of water-bearing rocks in aquifers can occur too. Studies have reported that when groundwater saturated with oxygen was pumped into exploitation wells in an in-situ drinking water production process, secondary minerals (as amorphous silica, clay, and rhodochrosite) were formed, whereas siderite dissolved and was redeposited (Strakhovenko et al., 2015; Kulakov et al., 2019). Nevertheless, there are not many studies that explain which unfavorable geochemical processes occur in LID rock-based filter materials, nor explain the mineralogical characteristics of the materials that contribute to improving or hindering their treatment capacity.

The main objective of this work is to identify the geochemical processes that occur between two model heavy metals (Mn^{2+} and Pb^{2+}), which are typically found in urban runoff, and chemical elements in the filter materials of an unvegetated LID system. By doing so, we aim to demonstrate the relationship between the mineralogy of the selected filter materials and the mobilization or removal capacity of toxic pollutants in LID systems.

2. Materials and methods

2.1. Description of filter materials

In filtration-based LID systems, different layers of materials with high hydraulic conductivity are used. Coarse materials are usually placed at the base to enhance water storage, while low water retention soil is added at the surface to sustain plant growth in vegetated systems. We therefore used the following filter materials (from bottom to top): tezontle (volcanic scoria), gravel, coarse sand, and soil. Tezontle is a cheap and abundant material that has been used for water depollution purposes (Yáñez-Ocampo et al., 2009; Tejeda et al., 2017), and it is one of the most used substrates for the production of vegetables and ornamental plants in Mexico (Ojodeagua-Arredondo et al., 2008). This configuration of materials can be used in several LID devices: if the upper layer is devoid of vegetation, the configuration of materials is adequate for infiltration trenches, which are shallow excavations filled with filter materials where runoff is temporarily stored for its subsequent percolation into the underlying soil (Lizárraga-Mendiola et al., 2017). As our experimental set-up was devoid of vegetation, infiltration trenches would be the LID system simulated more closely by our configuration of filter materials. By contrast, if a plant layer was added at the top, then the system can mimic a bioretention cell, a rain garden or a vegetated swale. In these cases, plants can lead to further modifications in the hydrological and mineralogical behavior of the LID systems that are still to be investigated.

Soil was obtained from the campus of the Universidad Autónoma del Estado de Hidalgo, Pachuca, Mexico; 20º05´39.97" N, 98º42´30.51" W). All other materials were obtained locally from exploitation banks, which formed at the same time and under the same geological processes of mineral ore deposits, located in the Pachuca-Real del Monte mining district. Since the sixteenth century, these ore deposits have produced fine Ag and Au, as well as base metals, mostly in the form of Fe, Zn, and Pb sulfides, with subordinate quantities of Cu (Clark, 1990). Fig. 1 shows the images of the filter materials obtained by scanning electronic microscopy (SEM) (JEOL/JSM-IT300, Japan).

Granulometric curves (Fig. 2) were constructed for each dry material from the particle-size distribution determined by mechanical sieve analysis (ASTM, 2007). The percentages of size-class fractions in a sample were determined using the ASTM C 1070–01 test (ASTM, 2014). For tezontle and gravel, the predominating size of particles was ~19 mm diameter. The most abundant particles in sand were ~2 mm diameter, whereas soil particles were predominantly < 0.6 mm diameter.

The soil used in the study was mainly composed of sand particles (63.3 %), followed by loam (24.9 %), and clay (11.8 %). The texture was evaluated according to ASTM (2007), and determined to be sandy loam according to the United States Department of Agriculture classification system (Soil Survey Division Staff, 2017). The method of Primo-Yúfera and Carrasco-Dorrién (1973) was used to assess the soil cation exchange capacity, which was 31.25 Cmol(+)/kg. The liquid limit and plastic limit of the soil were 19.00 % and 15.94 %, respectively, and were measured following ASTM D4318-10 (ASTM, 2010). These values indicate that the soil is semi-permeable and slightly plastic. As the plasticity index was 3.06 %, the Casagrande chart suggests the presence of low-plasticity clays (ML/CL; ASTM, 2010). The soil can be considered to be highly friable and of a soft consistency.

2.2. Synthetic urban runoff infiltration

The infiltration experiment was carried out in a 67 mm diameter glass column with a depth of 372 mm for holding filter media. From bottom to top, the column was filled with tezontle (56 mm), gravel (167 mm), coarse sand (56 mm), and soil (93 mm), which were

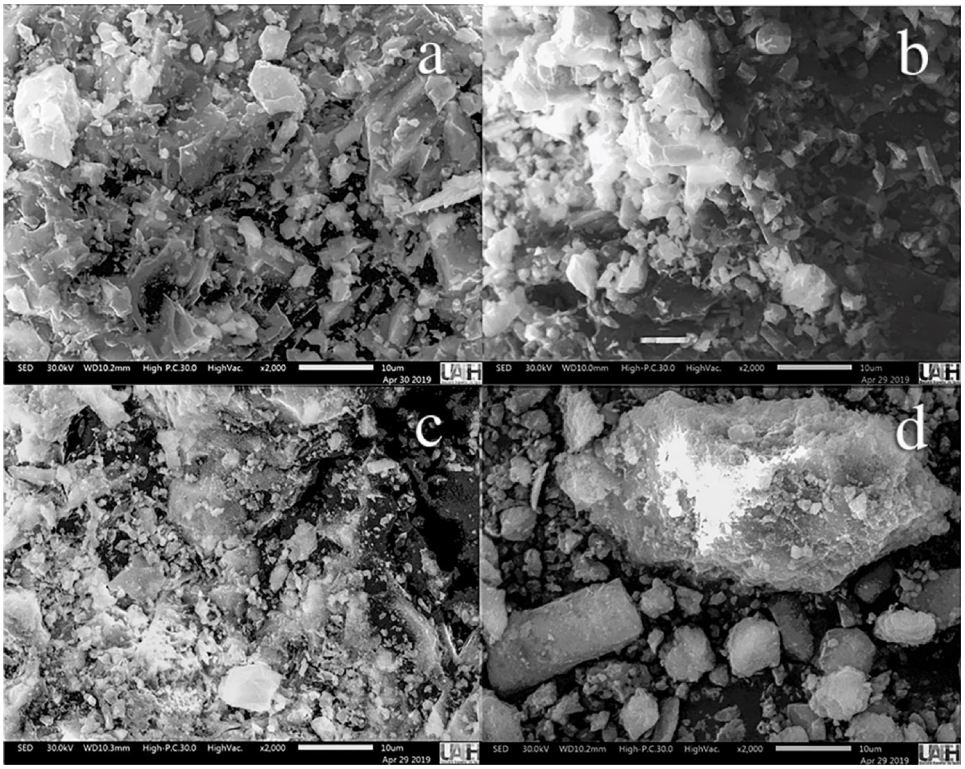

Fig. 1. Scanning electronic micrographs of the filter materials. a) tezontle (volcanic scoria), b) gravel, c) coarse sand, and d) soil.

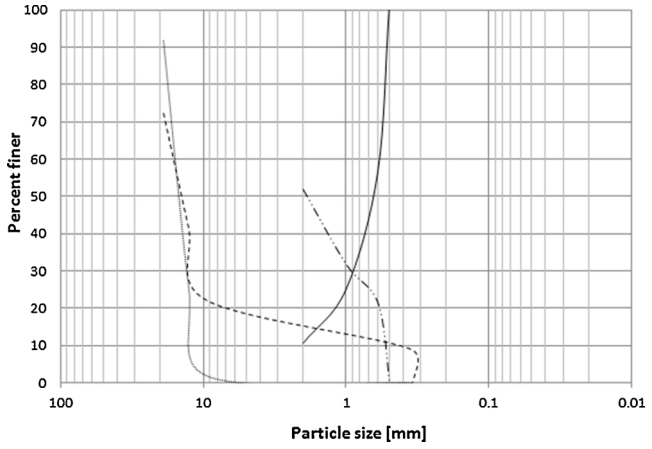

Fig. 2. Grain size distribution of the filter materials. The solid grey line is tezontle, the dashed line is gravel, the dash-dot line is coarse sand, and the solid black line is soil.

described in Section 2.1 (Fig. 1).

A synthetic urban runoff (SUR) was prepared using known volumes of $PbSO_4$ and $MnSO_4{\cdot}H_2O$ concentrated stock solutions (1000 mg/L each). To prepare 1 L of SUR, 1 mL of each stock solution were added to 998 mL of commercial bottled water to yield target concentrations of 1 mg Pb^{2+}/L and 1 mg Mn^{2+}/L, which simulate realistic concentrations in local runoff at the beginning of the rainy season in Pachuca, Mexico (Ortiz-Hernández et al., 2016). The column was operated in sequencing batch cycles through the feeding over 8 h of a constant flow of SUR (99 mL/h) by means of a peristaltic pump (Masterflex, USA). Roughly, after an 8 -h SUR feeding, the pump was stopped for the next 16 h with the purpose of recovering the total volume of infiltrated runoff, and then restarting one cycle every 24 h. The applied runoff flow in each cycle is equivalent to a rainfall rate of 28 mm/h, which is the maximum hourly rainfall registered during the rainy season (from April to November) for Pachuca between 1951–2010 (SMN, 2017). An 8 h feeding period used in our column experiment therefore corresponds to a simulated rain depth of 224 mm, which is the average maximum monthly rainfall for Pachuca between 1951–2010 (SMN, 2017).

Five 8 h replicate cycles were performed through the same filter column. In all of them, SUR prepared as specified above was fed. Triplicate samples from the inlet and outlet were taken to check reproducibility of analyses. Inlet samples were taken at the beginning of each 8 h cycle, whereas outlet samples were obtained only at the end of each 8 h cycle, when the fed water had passed through the column. The temperature and pH of each sample was measured (Hanna Instruments pH 210, USA). All samples were analyzed for major anions (HCO_3^-, CO_3^{2-}, Cl^-, and SO_4^{2-}), major cations (Ca^{2+}, Mg^{2+}, Na^+, and K^+), Mn^{2+}, and Pb^{2+}. HCO_3^-, CO_3^{2-}, and Cl^- were measured using titrimetric methods (2320-B and 4500-B; APHA, 2012). SO_4^{2-} was analyzed using a turbidimetric technique (4500-E; APHA, 2012). The concentrations of major cations, Mn^{2+}, and Pb^{2+} were determined by flame atomic absorption spectrometry using a SpectrAA spectrophotometer (Varian 880, USA).

Water quality variables at the inlet and outlet of the column were compared using a two-sided paired Fisher test in Minitab 16 (Minitab Inc., State College, PA, USA). A significance level of $\alpha = 0.05$ was used for all statistical tests.

2.3. Geochemical modeling

Geochemical modeling was performed using the PHREEQC software (Parkhurst and Appelo, 2013), which uses ion-association and Debye Hückel expressions to account for the non-ideality of aqueous solutions (Kim et al., 2008). The software includes databases used for speciation calculations based on the approach of the law of mass action, which determines the ionic activities at equilibrium (Eq. (1)).

$$lnK_m = \sum_{i=1}^{N} \nu_{mi} ln\alpha_i \quad (m=1,...,M), \tag{1}$$

where K_m is the equilibrium constant of the *m*th reaction, ν_{mi} is the stoichiometric coefficient of the *i*th species in the *m*th reaction, and negative ν_{mi} is used for reactants and positive ν_{mi} is used for products (Leal et al., 2016). Several interactions may affect speciation: soluble species, precipitates of solid phases, oxidation states, complexes, among others (Magu et al., 2016). Within one-time step during the simulation, geochemical equilibrium reactions are calculated, and then kinetic reactions for every cell in the simulation domain are modeled. This type of aqueous model is adequate for low ionic strength solutions (e.g., fresh water) (Lipiec, 2017).

The saturation indices (SIs) of infiltrated water with respect to the different minerals contained in the filter materials were assessed for each infiltration cycle, and were calculated for several possible reactions as determined by Eq. (2):

$$SI = \log[IAP/K_T], \quad (2)$$

where SI is the saturation index, IAP is the ion activity product calculated based on the water analyses (although it is assumed that a real solution may not be in equilibrium), and K_T is the equilibrium constant of the reaction. If SI is zero, the aqueous solution is considered to be at equilibrium. SI < 0 indicates a state of under-saturation (or dissolution), while SI > 0 for an aqueous solution indicates over-saturation (or precipitation) (Appelo and Postma, 2005). Further information is provided by Magu et al. (2016).

Pearson correlation coefficients were calculated to identify the potential relationships between mineral groups. The calculations were performed using Minitab 16.

2.4. Mineralogical characterization of the filter materials

The identification of mineral phases in the filter materials was carried out by powder X-ray diffraction (PXRD) (INEL Equinox 2000). The diffractometer was used with an X-ray tube of cobalt anode operating at 30 mA and 25 kV. Samples obtained after the SUR infiltration tests and samples that had not been in contact with the SUR were air-dried at room temperature (~21 °C) to eliminate humidity. Samples were powdered with an agate mortar and carefully transferred into an aluminum circular sample holder (ϕ = 10 mm, 2 mm depth) that was horizontally placed in the center of the diffractometer's goniometer (ϕ = 185 mm). Debye-Scherrer geometry and reflection configuration was used; the detector consisted of a curve position sensitive (CPS) detector that covered an angular range of 110°. The simultaneous detection of the whole of the 2θ Bragg range of this detector was divided into 4096 channels, thus resulting in an average step size of 0.031°. Every experiment was scanned from ~5° to ~120° 2θ using CoKα1 radiation obtained through a Ge-monochromator situated at the primary beam, thereby allowing the experimental stripping of the Kα2 line.

These experimental conditions and the geometry features of the diffractometer assure sufficient representation of the diffracted planes to optimize the identification of mineral phases within, a priori, complex geological samples (i.e., soils, sands, volcanic scoria, and gravel).

The identification of mineral phases was performed by a combination of automatic and manual peak searches based on the powder diffraction file data base (version 4 +, released by the International Centre for Diffraction Data) and were implemented in the Jade 6.5 program (Lilli et al., 2019).

3. Results

3.1. SUR infiltration tests

The means (and standard deviations) measured in the SUR before and after the five 8 h infiltrations are presented in Table 1 along with the Mexican drinking water quality standards (NOM, 2000) for comparison purposes. Although the same SUR was fed in each cycle, unexpectedly high concentrations of some ions were detected in the outlet, and only in certain cycles. For instance, in one of the cycles, the Pb^{2+} concentration of the column outlet was even higher than the concentration of the inlet. To take into account this fact, the maximum values measured for each SUR constituent at the column outlet are also included in Table 1. Since the SUR was prepared with commercial bottled water, the concentrations of Ca^{2+}, K^+, and Cl^- in the SUR before the infiltration were below the limit of detection for the analytical techniques used in this study. Considering the mean values of the five 8 h cycles, the concentrations of these ions increased after column infiltration and were detectable in the post-filtrate solution. Mean values (of the five 8 h cycles) of total alkalinity, and the HCO_3^- and Mg^{2+} concentrations also increased after column infiltration, whereas the mean values of pH and temperature, and the mean concentrations of SO_4^{2-}, Na^+, Mn^{2+}, and Pb^{2+} diminished. CO_3^{2-} ions were not detected in the SUR at the inlet or the outlet. Filter materials modified the SUR composition in a significant way, because, with the exception of temperature, Mn^{2+}, and Pb^{2+}, other mean concentrations in the SUR at the inlet were significantly different ($p < 0.05$) from those at the outlet (considered as the mean values of the five 8 h cycles).

Before infiltration, Mn^{2+} and Pb^{2+} concentrations in the SUR exceeded the Mexican drinking water quality standard of 0.15 mg Mn/L and 0.01 mg Pb/L (NOM, 2000). As mentioned, we used Mn and Pb concentrations that were representative of those previously measured in local runoff at the beginning of the rainy season. This seasonal "first-flush" effect results in highly polluted streams due to the length of the preceding dry period (Ortiz-Hernández et al., 2016), and often leads to concentrations of metals exceeding Mexican drinking water quality standards and even wastewater discharge limits, for example, > 0.2–1 mg Pb/L (NOM, 2018). However, although the mean Mn^{2+} and Pb^{2+} concentrations in the SUR diminished at the outlet, the reductions were not statistically significant ($p > 0.05$), and concentrations were still in excess of drinking water standards (Table 1).

Based on the relative dominance of major cations and anions in Piper diagrams, two types of hydrochemical facies were identified in the SUR before and after passing through the column (Fig. 3). The SUR composition at the column inlet was predominantly of a SO_4-Mg type water, whereas after being in contact with the filter materials the SUR composition was predominately of a SO_4-Mg-Ca type water.

3.2. Geochemical modeling

Some geochemical processes such as precipitation (over-saturation) or dissolution (under-saturation) can occur in LID systems. Precipitation may contribute to heavy metals immobilization, particularly in the case of contaminated infiltration water, whereas dissolution may lead to the mobilization of heavy metals (Stumm, 1992).

The inlet SUR solution had an ionic strength (I) of 0.2163 mol/kg, and an electrical balance of -0.276 eq. (error 1.11 %). From the maximum values of the SUR constituents (Table 1) recovered at the outlet after passing through the filter we obtained a simulated solution with similar ionic strength (0.205 mol/kg) and electrical balance (-0.28 eq., error 4.15 %) to the inlet solution.

The results obtained using the PHREEQC database and software (Parkhurst and Appelo, 2013) indicated the interactions between the SUR and the filter materials. These calculations assumed that the dissolved species in the infiltrated water were at chemical equilibrium with the filter materials. When the solution enters to the filter, no chemical reaction intervening in its composition has occurred yet. However, at a certain point, this equilibrium ends and the geochemical exchange between the infiltrated water and the minerals ensues. This exchange can lead to a dissolution or to a precipitation affecting the water quality in a favorable or unfavorable way.

As mentioned above, some ion concentrations decreased slightly at the outlet (SO_4^{2-}, Na^+, Mn^{2+}, and Pb^{2+}), whereas Mg^{2+} increased and others were detected only at the outlet (Cl- and Ca^{2+}) and not at the inlet. Hence, the geochemical interactions were focused on sulfates,

Table 1
Physicochemical composition of synthetic urban runoff (SUR) measured at the inlet and the outlet of the infiltration column and Mexican drinking water quality standards.

	Mean inlet values (SD)[A]	Mean outlet values (SD)[A]	Maximum outlet values [B]	Drinking water standard [C]
pH	7.5 (0.01)	6.36 (0.17)	6.5	6.5 – 8.5
Temperature [°C]	21.3 (2.22)	19.8 (1.30)	21	–
Total alkalinity [mg $CaCO_3$/L]	128.83 (0.84)	177.24 (12.32)	195.32	–
HCO_3^- [mg/L]	157.18 (1.02)	216.23 (15.03)	238.29	–
Cl^- [mg/L]	< DL	0.006 (0.002)	0.0087	250
SO_4^{2-} [mg/L]	76.03 (1.02)	56.57 (6.46)	66.0	400
Na^+ [mg/L]	1.032 (0.01)	0.422 (0.024)	0.45	200
Ca^{2+} [mg/L]	< DL	0.218 (0.008)	0.23	–
K^+ [mg/L]	< DL	5.476 (0.424)	6	–
Mg^{2+} [mg/L]	0.052 (0.002)	0.336 (0.011)	0.35	–
Mn^{2+} [mg/L]	0.913 (0.002)	0.782 (0.261)	0.940	0.15
Pb^{2+} [mg/L]	0.943 (0.018)	0.678 (0.588)	1.185	0.01

DL = Detection limit.
[A] n = 15, standard deviation values are shown in parentheses.
[B] Mean values were calculated from the maximum triplicates, n = 3.
[C] NOM (2000).

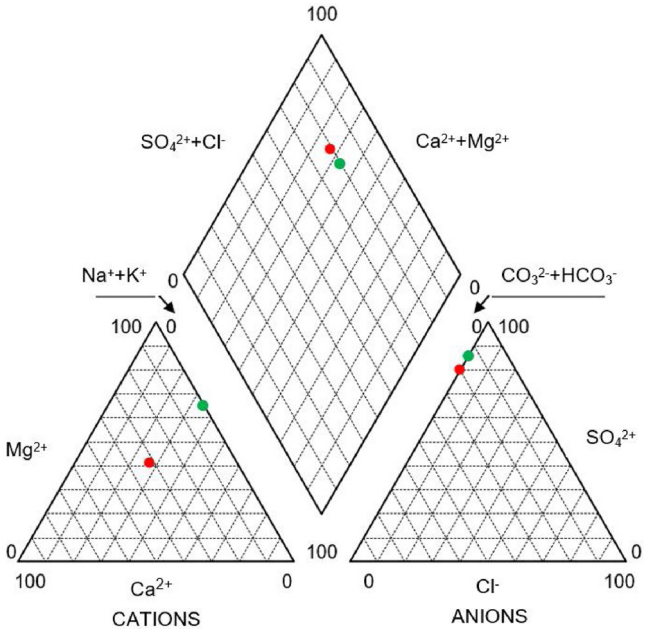

Fig. 3. Piper diagram of the inlet (green points) and the outlet (red points) synthetic urban runoff composition.

Table 2
Maximum saturation indices (SIs) calculated at the inlet and the outlet of the infiltration column.

Phase	Maximum SIs inlet values	Maximum SIs outlet values
Sulfates		
Anglesite ($PbSO_4$)	−0.52	0.65
Epsomite ($MgSO_4{\cdot}7H_2O$)	–	−2.11
Lanarkite ($Pb_2O(SO_4)$)	–	−1.78
Carbonates		
Calcite ($CaCO_3$)	−1.7	−1.26
Rhodochrosite ($MnCO_3$)	–	1.97
Oxides		
Hausmannite (Mn_3O_4)	−7.46	−18.66
Manganite (MnOOH)	−3.32	−7.39
Chlorides		
Sylvite (KCl)	–	−8.59

carbonates, oxides, and chloride mineral groups. Independently of the oscillation of the water quality, the SIs calculated for these mineral groups were similar over the five infiltration cycles. Therefore, we discussed only the maximum values obtained at the inlet and outlet of the column (Table 2).

At the inlet, the SUR solution was under-saturated with respect to lead sulfate (anglesite), carbonates (calcite), and manganese oxides (hausmannite > manganite). At the outlet, the simulated SUR solution (e.g., the solution having the maximum values of all its constituents) showed the following geochemical behavior: anglesite oscillated between a state of under-saturation and over-saturation, whereby the over-saturated state had the highest SI value (0.65). In addition, two new sulfates (epsomite < lanarkite) appeared at an under-saturated state (as secondary minerals). Manganese oxides (hausmannite > manganite) maintained their under-saturated state, although their SIs decreased slightly. Other carbonates such as calcite (under-saturated state) and rhodochrosite (as a secondary mineral, over-saturated state) were identified. The presence of chlorides such as sylvite (under-saturated state) was also determined after the maximum values simulated at the outlet.

The identification of correlations between the minerals as indicated by the geochemical model can reveal the behavior and origin of solutes and the processes that generated the observed water composition (Sánchez-Salcedo et al., 2017). A direct correlation exists when an increase or decrease in the value of one parameter is associated with a corresponding increase or decrease in the value of another parameter. If the correlation coefficient (r) > 0.7, two parameters were considered to be strongly correlated at a significance level p = 0.05 (Table 3).

From Table 3, when the SI of anglesite increased and became over-saturated, minerals such as calcite > lanarkite > sylvite decreased and became under-saturated. On the contrary, when anglesite decreased its SI and became under-saturated, these other minerals increased. In the case of calcite, its under-saturation corresponded to the under-saturation of manganese oxides (hausmannite > manganite), thus favoring the formation of a secondary mineral (rhodochrosite) and the under-saturation of chlorides (sylvite). On the other hand, manganese oxides (hausmannite > manganite) correlated almost perfectly with each other (under-saturated state).

3.3. PXRD results

Fig. 4a–d show the diffractograms (ordered from top to bottom of the infiltration column) of soil, coarse sand, gravel, and tezontle (volcanic scoria). Each diffractogram provides a comparison of each material before and after contact with the SUR. In general, the resolution

Table 3
Correlation matrix among the mineral constituents for the infiltration column simulation (coefficients > 0.7 are shown in bold).

	Anglesite ($PbSO_4$)	Epsomite ($MgSO_4{\cdot}7H_2O$)	Lanarkite ($Pb_2O(SO_4)$)	Calcite ($CaCO_3$)	Rhodochrosite ($MnCO_3$)	Hausmannite (Mn_3O_4)	Manganite (MnOOH)	Sylvite (KCl)
Anglesite ($PbSO_4$)	1.00							
Epsomite ($MgSO_4{\cdot}7H_2O$)	−0.36	1.00						
Lanarkite ($Pb_2O(SO_4)$)	**−0.79**	0.45	1.00					
Calcite ($CaCO_3$)	**−0.75**	−0.01	0.20	1.00				
Rhodochrosite ($MnCO_3$)	−0.42	−0.49	−0.49	0.66	1.00			
Hausmannite (Mn_3O_4)	−0.18	−0.26	−0.32	**0.85**	**0.85**	1.00		
Manganite (MnOOH)	−0.23	−0.28	−0.13	**0.92**	**0.92**	**0.99**	1.00	
Sylvite (KCl)	**−0.87**	0.51	0.48	**0.85**	**0.85**	0.56	0.63	1.00

and optics of the diffractometry technique resulted in 2θ-I data that serve to identify a great number of phases in each of the diffractograms. Although differences between both types of diffractograms are not easy to appreciate, an accurate study of overlapping peaks along with previous knowledge of the whole rock and SUR chemistry allow us to make some inferences.

Samples of soil (uppermost or surface layer in the filter column) showed more mineralogical differences in comparison to the rest of the filter materials. The presence of a clay fraction (including illite, kaolinite, and mixed clay kaolinite-montmorillonite), Mn-bearing oxides, and the only carbonate of the filter system (calcite) were the most relevant differences in this layer before the infiltration of the SUR (i.e., virgin soil; Fig. 4a). As the geochemical model indicated, the supply of Ca^{2+} in the column outlet originated from the dissolution of calcite in the soil by the infiltrating SUR. The formation of another carbonate (rhodochrosite) was the result of the combination of Mn^{2+} from the SUR and $CO_3{}^{2-}$ from the decomposition of the original calcite. The other Mn species were identified as dissolution products based on the SUR composition at the column outlet. Originally, these latter phases only belonged to the oxide group: hausmannite and manganite, and were only represented in the soil layer of the filter. Partial dissolution of calcite and Mn oxides (refer to Fig. 4a differences in peak intensities between the two patterns) allowed the formation of Mn carbonate (rhodochrosite). Thus, principal diffracted peaks of these oxides and calcite remained after the SUR infiltration. With regards to the peaks that represent quartz and albite (pure Na or very Na-rich plagioclase feldspar), no changes were observed and these are considered as fixed minerals or, in other words, reference silicates for all the layers of the filter. In the case of clay minerals, which are also silicates, a constant intensity of the diffracted peaks is not straightforward to corroborate because of the usual preference for an orientational trend in phyllosilicates.

Besides quartz and albite (common phases in all filter materials), lanarkite, barite, and anglesite conformed to their common mineralogy in the three inferior layers (i.e., coarse sand, gravel, and tezontle). All of these latter sulfates are solid reservoirs for Pb and Ba. On the one hand, the PXRD patterns of coarse sand (Fig. 4b), both before and after contact with SUR, did not differ in their relative intensities of these phases,

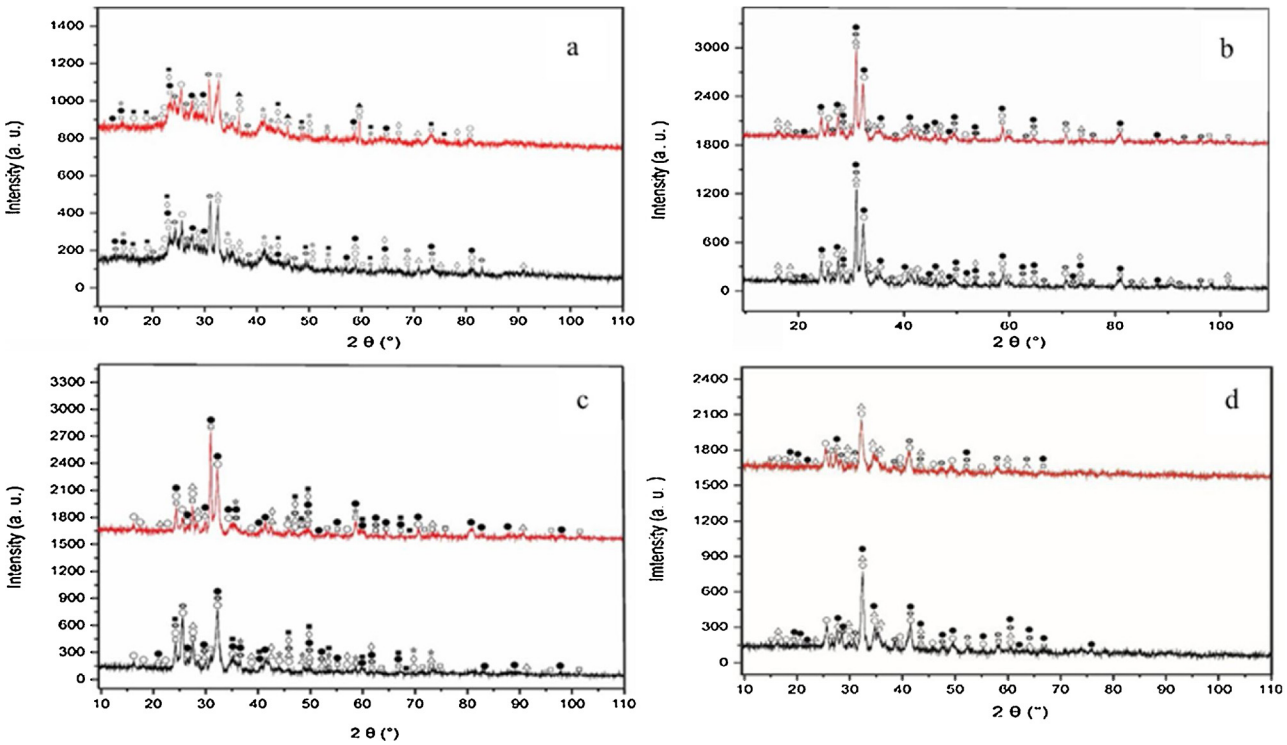

Fig. 4. Powder X-ray diffraction diagrams for samples (ordered from top to bottom of the filter column). (a) Virgin soil (black) and soil infiltrated by synthetic urban runoff (red), where □: Quartz; ○: Albite; △: Hausmannite; ☼: Manganite; ●: Calcite; ◊: Illite; ☆: Kaolinite; ■: Kaolinite-montmorillonite; ▲: Rhodochrosite. (b) Virgin coarse sand (black) and coarse sand infiltrated by synthetic urban runoff (red), where □: Quartz; ○: Albite; △: Lanarkite; ☼: Barite; ●: Anglesite; ◊: Sylvite. (c) Virgin gravel (black) and gravel infiltrated by synthetic urban runoff (red), where □: Quartz; ○: Albite; △: Lanarkite; ☼: Barite; ●: Anglesite; ◊: Sylvite; ☆: Mendipite; ■: Epsomite. (d) Virgin tezontle (black) and tezontle infiltrated by synthetic urban runoff (red). □: Quartz; ○: Albite; △: Lanarkite; ☼: Barite; ●: Anglesite.

which is consistent with the low solubility of sulfates. On the other hand, the gravel samples showed relatively large differences in the solubility of sulfates. In fact, Pb sulfates were found to precipitate in this layer (e.g., the evolution of the peak of anglesite in Fig. 4c), thereby increasing the weight fraction of preexisting anglesite and lanarkite after infiltration. In the same layer, epsomite was notably dissolved due to SUR infiltration, and this scenario is the only explanation to justify the increase in the Mg concentration at the column outlet. Similarly, although we did not measure the Ba concentration, the barite presence in the gravel is suggested as the only source of Ba at the outlet. This is corroborated by the significant decrease in the principal diffracted peak in the infiltrated gravel (Fig. 4c). It is worth noting that Ba is also a toxic metal, and its presence in the gravel layer is an indication of the hazard derived from the use of this material in LID filters. Due to its potential effect on human blood pressure, Ba concentrations higher than the World Health Organization guideline value (i.e., 1.3 mg/L) are considered unsafe (WHO, 2016).

Tezontle (volcanic scoria), the most inferior layer of the filter, showed an inverse behavior with respect to Pb sulfates, as the solubility of these minerals is very clear in the PXRD patterns (Fig. 4d). Both anglesite and lanarkite dissolved when the SUR passed through this layer. Thus, the tezontle layer is a source of Pb; however, this Pb input is still lower than the removal that occurred in the upper layer, and the outlet SUR was found to have a slightly lower Pb concentration than of that in the inlet SUR. Consequently, by considering the opposite effects of gravel and tezontle on the precipitation/dissolution of Pb sulfates, we conclude that the effects of particle size and porosity were determinants in the geochemical exchange of Pb in our experiment.

3.4. Interactions between SUR and filter materials

Infiltration-based LID systems are well known for their ability to treat urban runoff water (Shrestha et al., 2018). In the present study, a model for metal geochemical processes was coupled to a chemical and mineralogical characterization method in order to determine the interactions between filter materials and urban runoff pollutants (Sánchez-Salcedo et al., 2017). In our study, the relationship between the mineral content of the materials used in the filter and their ability to remove or mobilize toxic pollutants from synthetic urban runoff was analyzed. Fig. 5 summarizes the geochemical exchanges that occurred between the mineral content of filter materials when they were exposed to SUR.

We found that the greatest variety of minerals were present in the soil layer. Among these minerals, Mn oxides (hausmannite > manganite) and carbonates (calcite) were dissolved, thus mobilizing Mn^{2+}, Ca^{2+} and CO_3^{2-}, respectively, towards the inferior layer. In the coarse sand layer, CO_3^{2-} and Mn^{2+} were mobilized from the soil layer, and then combined to form an endogenous, new secondary mineral (rhodochrosite) by means of precipitation (Strakhovenko et al., 2015). Mn^{2+} that was not combined with carbonates (possibly from hausmannite, since it was the mineral that had the highest under-saturated state), as well as Ca^{2+}, continued to move towards the inferior layers. In the coarse sand layer, chlorides were also dissolved, and the K^+ and Cl- ions were mobilized towards the lower layers.

Several geochemical processes occurred in the gravel layer. Pb sulfates (lanarkite > epsomite > barite) became dissolved and favored the mobilization of Pb^{2+}, Mg^{2+}, and possibly Ba^{2+}, respectively. In this same layer, another Pb sulfate (anglesite) was over-saturated, thus favoring the precipitation of Pb (Marani et al., 1995). Meanwhile, the chlorides were also dissolved, and again K^+ and Cl^- were mobilized. In the most inferior layer of volcanic scoria (i.e., tezontle), dissolution of sulfates occurred again (anglesite > lanarkite) and mobilized Pb^{2+} to the natural substrate.

Among the metal geochemical processes potentially occurring in the filter materials, our model included those occurring between pollutants commonly present in real urban runoff (Ortiz-Hernández et al., 2016).

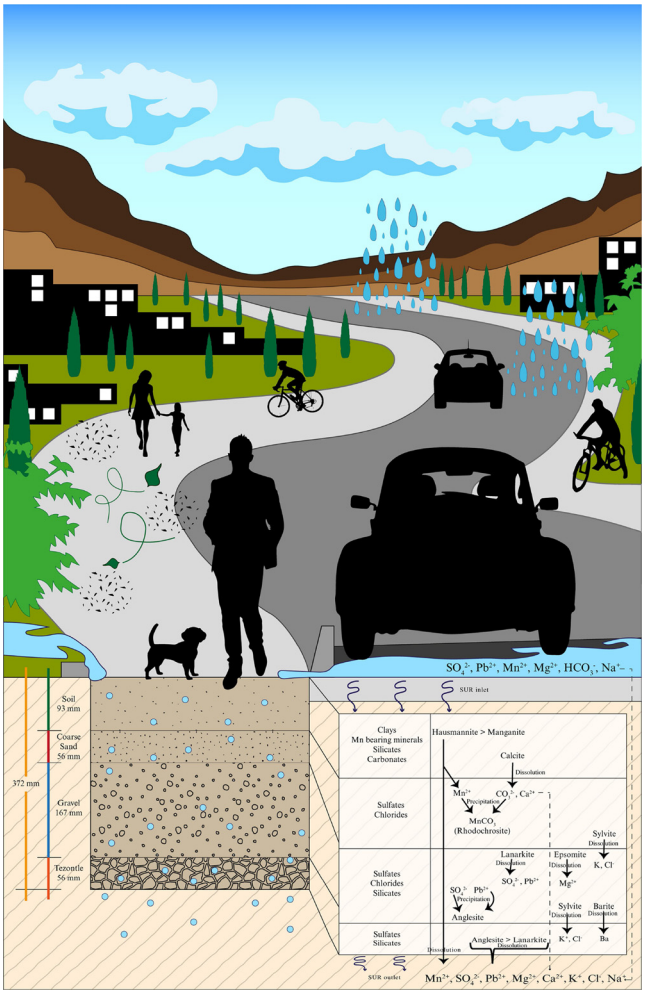

Fig. 5. Geochemical modeled interactions between urban runoff pollutants and the filter materials.

We found that not only did the filter have a removal capacity for some elements, but also acted as a source of geogenic contaminants. This induced geogenic pollution allows us to hypothesize that the expected filter treatment capacity was altered by the geochemical exchanges that occurred between minerals in the filter materials and the synthetic urban runoff.

4. Conclusions

This study highlights the importance of characterizing the mineral composition of filter materials prior to their use in an unvegetated LID system. The materials employed in our filter came from a bank formed from a metallic ore deposit where Ag, Au, and base metals have been exploited. This geological origin resulted in a variety of minerals that interacted with the SUR pollutants in the column experiment. We identified the presence of toxic pollutants such as Pb^{2+}, and Mn^{2+} in the filter outlet, which came partially from the inlet SUR but also from the filter material itself. We hypothesize also the presence of Ba^{2+} in the infiltrated SUR (due to the confirmed presence of barite in sand, gravel, and tezontle), but we did not actually measure it. Geochemical modeling indicated that the main intervening process was mineral under-saturation (dissolution), which added new ions to the infiltrating water (Cl^- and Ca^{2+}) and also increased the contents of other ions contained in the SUR (Mn^{2+}, Pb^{2+}, Mg^{2+}, Ca^{2+}, and K^+). We conclude that it is important to know the mineral composition of materials selected for use in LID systems as a means of determining any unfavorable

geochemical interactions, and therefore preventing the addition of contaminants to infiltrating runoff. Furthermore, the determination of the possible geochemical interactions that occur between a filter and runoff water allows a better understanding of the mechanisms involved in runoff pollution removal.

A limitation of this study was the evaluation of only one SUR pH value (7.5). It would therefore be useful to carry out additional experiments to assess the effect of acidic or alkaline pH values on the mobilization of toxic metals. Better yet, these results should be validated in a real-scale LID system, where pH fluctuations are likely to occur and a higher filter height could modify the outcomes of this study.

Based on the results of this study, it is advisable to further explore the effect of the following variables on the geochemical exchange between urban runoff and the filter materials in an unvegetated LID: a) the urban runoff pH; b) the height of the column and the granulometry of the materials; c) the presence of other metals of interest (Cr, Cu, Ni, Zn, As, Hg, Ni, Cd, or Ba) at the inlet and outlet of the filter column. As well, the characterization of materials to be used in the filter in terms of elementary analysis by scanning electron microscopy might be insightful.

Funding

This research did not receive any specific grant from funding agencies in the public, commercial, or not-for-profit sectors.

CRediT authorship contribution statement

Marcelino Antonio Zúñiga-Estrada: Investigation, Methodology. **Gabriela A. Vázquez-Rodríguez:** Data curation, Writing - original draft, Writing - review & editing. **Màrius Ramírez-Cardona:** Formal analysis, Data curation. **Liliana Lizárraga-Mendiola:** Conceptualization, Data curation, Writing - original draft.

Declaration of Competing Interest

None.

Acknowledgements

Marcelino Antonio Zúñiga-Estrada acknowledges the PhD scholarship provided by the Consejo Nacional de Ciencia y Tecnología (CONACYT-Mexico). All the authors thank the insightful comments and help of Dr. Azdrúbal Lobo-Guerrero concerning the interpretation of the PXRD results. The authors would like to thank the reviewers and editors for their comments which helped in improving the manuscript.

Appendix A. Supplementary data

Supplementary material related to this article can be found, in the online version, at doi:https://doi.org/10.1016/j.jhazmat.2020.122136.

References

APHA, 2012. Standard Methods for the Examination of Water and Wastewater, 22nd ed. American Public Health Association/American Water Works Association/Water Environment Federation, Washington D.C.

Appelo, C.A.J., Postma, D., 2005. Geochemistry, Groundwater and Pollution, second ed. CRC Press, Amsterdam.

ASTM C1070-01, 2014. Standard Test Method for Determining Particle Size Distribution of Alumina or Quartz by Laser Light Scattering. ASTM International, West Conshohocken, PA. https://doi.org/10.1520/C1070-01R14. www.astm.org.

ASTM D422-63, 2007. Standard Test Method for Particle-Size Analysis of Soils (Withdrawn 2016). ASTM International, West Conshohocken, PA. https://doi.org/10.1520/D0422-63R07E02. www.astm.org.

ASTM D4318-10, 2010. Standard Test Methods for Liquid Limit, Plastic Limit, and Plasticity Index of Soils. ASTM International, West Conshohocken, PA. https://doi.org/10.1520/D4318-10. www.astm.org.

Clark, K.F., 1990. Mexican silver deposits. Society of Economic Deposits Guidebook Series Vol. 6https://doi.org/10.5382/GB.06.

Goulden, S., Portman, M.E., Carmon, N., Alon-Mozes, T., 2018. From conventional drainage to sustainable stormwater management: beyond the technical challenges. J. Environ. Manage. 219, 37–45. https://doi.org/10.1016/j.jenvman.2018.04.066.

Ivanovsky, A., Belles, A., Criquet, J., Dumoulin, D., Noble, P., Alary, C., Billon, G., 2018. Assessment of the treatment efficiency of an urban stormwater pond and its impact on the natural downstream watercourse. J. Environ. Manage. 226, 120–130. https://doi.org/10.1016/j.jenvman.2018.08.015.

Kabir, M.I., Daly, E., Maggi, F., 2017. Geochemical modelling of heavy metals in urban stormwater biofilters. Ecol. Eng. 102, 565–576. https://doi.org/10.1016/j.ecoleng.2017.02.064.

Kim, S.S., Baik, M.H., Kang, K.C., Kwon, S.H., Choi, J.W., 2008. Solubilities of actinides in a domestic groundwater and a bentonite porewater calculated by using PHREEQC. J. Ind. Eng. Chem. 14 (6), 739–746. https://doi.org/10.1016/j.jiec.2008.07.005.

Kulakov, V.V., Berdnikov, N.V., Krutikova, V.O., Arkhipova, E.E., 2019. Natural and technogenic mineral formation in the aquifer of the Amur-Tunguska interfluves. Russ. J. Pacific Geol. 13 (2), 154–162. https://doi.org/10.1134/S1819714019020064.

Lau, A.Y., Tsang, D.C., Graham, N.J., Ok, Y.S., Yang, X., Li, X.D., 2017. Surface-modified biochar in a bioretention system for *Escherichia coli* removal from stormwater. Chemosphere 169, 89–98. https://doi.org/10.1016/j.chemosphere.2016.11.048.

Leal, A.M.M., Kulik, D.A., Saar, M.O., 2016. Enabling Gibbs energy minimization algorithms to use equilibrium constants of reactions in multiphase equilibrium calculations. Chem. Geol. 437, 170–181. https://doi.org/10.1016/j.chemgeo.2016.05.029.

Lilli, M.A., Nikolaidis, N.P., Karatzas, G.P., Kalogerakis, N., 2019. Identifying the controlling mechanism of geogenic origin chromium release in soils. J. Hazard. Mater. 366, 169–176. https://doi.org/10.1016/j.jhazmat.2018.11.090.

Lipiec, I., 2017. Assessment of hydrogeochemical equilibrium in the sulphurous water - rock environment in the Solec-Zdrój area. Procedia Earth Planet. Sci. 17, 225–228. https://doi.org/10.1016/j.proeps.2016.12.077.

Lizárraga-Mendiola, L., Vázquez-Rodríguez, G., Lucho-Constantino, C., Bigurra-Alzati, C., Beltrán-Hernández, R., Ortiz-Hernández, J., López-León, L., 2017. Hydrological design of two low-impact development techniques in a semi-arid climate zone of Central Mexico. Water (Switzerland) 9 (8), 561. https://doi.org/10.3390/w9080561.

Magu, M.M., Govender, P.P., Ngila, J.C., 2016. Geochemical modelling and speciation studies of metal pollutants present in selected water systems in South Africa. Phys. Chem. Earth 92, 44–51. https://doi.org/10.1016/j.pce.2015.08.001.

Marani, D., Macchi, G., Pagano, M., 1995. Lead precipitation in the presence of sulphate and carbonate: testing of thermodynamic predictions. Water Res. 29 (4), 1085–1092. https://doi.org/10.1016/0043-1354(94)00232-V.

Mohanty, S.K., Valenca, R., Berger, A.W., Iris, K.M., Xiong, X., Saunders, T.M., Tsang, D.C., 2018. Plenty of room for carbon on the ground: potential applications of biochar for stormwater treatment. Sci. Total Environ. 625, 1644–1658. https://doi.org/10.1016/j.scitotenv.2018.01.037.

Monrabal-Martínez, C., Aberle, J., Muthanna, T.M., Orts-Zamorano, M., 2018. Hydrological benefits of filtering swales for metal removal. Water Res. 145, 509–517. https://doi.org/10.1016/j.watres.2018.08.051.

Nguyen, T.T., Ngo, H.H., Guo, W., Wang, X.C., Ren, N., Li, G., Ding, J., Liang, H., 2019. Implementation of a specific urban water management - Sponge City. Sci. Total Environ. 652, 147–162. https://doi.org/10.1016/j.scitotenv.2018.10.168.

NOM, 2000. Modificación a la Norma Oficial Mexicana NOM-127-SSA1-1994, Salud ambiental. Agua para uso y consumo humano. Límites permisibles de calidad y tratamientos a que debe someterse el agua para su potabilización. Modified guidelines for drinking water and treatments to be applied [in Spanish]. Secretaría de Salud, México (Accessed 19 August 2019). http://www.salud.gob.mx/unidades/cdi/nom/m127ssa14.html.

NOM, 2018. Proyecto de Modificación a la Norma Oficial Mexicana NOM-001-SEMARNAT-1996. Que establece los límites máximos permisibles de contaminantes en las descargas de aguas residuales en aguas y bienes nacionales. Modified guidelines for raw water discharges and national reservoirs. Secretaría de Medio Ambiente y Recursos Naturales, México (Accessed 11 September 2019). https://agua.org.mx/wp-content/uploads/2018/02/Proyecto-de-Modificacion-NOM-001-SEMARNAT-1996-13Dic2017.pdf.

Ojodeagua-Arredondo, J.L., Castellanos-Ramos, J.Z., Muñoz-Ramos, J.J., Alcántar-González, G., Tijerina-Chávez, L., Vargas-Tapia, P., Enríquez-Reyes, S., 2008. Eficiencia de suelo y tezontle en sistemas de producción de tomate en invernadero [in Spanish]. Revista Fitotecnia Mexicana 31 (4), 367–374.

Ortega-Villar, R., Lizárraga-Mendiola, L., Coronel-Olivares, C., López-León, L.D., Bigurra-Alzati, C.A., Vázquez-Rodríguez, G.A., 2019. Effect of photocatalytic Fe_2O_3 nanoparticles on urban runoff pollutant removal by permeable concrete. J. Environ. Manage. 242, 487–495. https://doi.org/10.1016/j.jenvman.2019.04.104.

Ortiz-Hernández, J., Lucho-Constantino, C., Lizárraga-Mendiola, L., Beltrán-Hernández, R.I., Coronel-Olivares, C., Vázquez-Rodríguez, G., 2016. Quality of urban runoff in wet and dry seasons: a case study in a semi-arid zone. Environ. Sci. Pollut. Res. - Int. 23 (24), 25156–25168. https://doi.org/10.1007/s11356-016-7547-7.

Page, D., Bekele, E., Vanderzalm, J., Sidhu, J., 2018. Managed aquifer recharge (MAR) in sustainable urban water management. Water (Switzerland) 10 (3), 1–16. https://doi.org/10.3390/w10030239.

Parkhurst, D.L., Appelo, C.A.J., 2013. Description of input and examples for PHREEQC version 3 — a computer program for speciation, batch-reaction, one-dimensional transport, and inverse geochemical calculations. U.S. Geological Survey Techniques and Methods. https://doi.org/10.1016/0029-6554(94)90020-5. Book 6, Chapter A43, 6-43A.

Primo-Yúfera, E., Carrasco-Dorrién, J.M., 1973. Química Agrícola I: Suelos y Fertilizantes [in Spanish]. Alhambra, Madrid. .

Robertson, W.D., Feng, D., Kobylinski, S., Finnigan, D.S., Merkley, C., Schiff, S.L., 2018.

Low cost media can filter particulate phosphorus from turbid stream water under short retention times. Ecol. Eng. 123, 95–102. https://doi.org/10.1016/j.ecoleng.2018.08.015.

Sánchez-Salcedo, E.R., Garrido-Hoyos, S.E., Esteller, M.V., Martínez-Morales, M., Ocampo-Astudillo, A., 2017. Hydrogeochemistry and water-rock interactions in the urban area of Puebla Valley aquifer (Mexico). J. Geochem. Explor. 181, 219–235. https://doi.org/10.1016/j.gexplo.2017.07.016.

Shrestha, P., Hurley, S.E., Wemple, B.C., 2018. Effects of different soil media, vegetation, and hydrologic treatments on nutrient and sediment removal in roadside bioretention systems. Ecol. Eng. 112, 116–131. https://doi.org/10.1016/j.ecoleng.2017.12.004.

SMN, 2017. Normales Climatológicas 1981-2000, Estación Pachuca, Hgo [in Spanish]. Servicio Meteorológico Nacional, Comisión Nacional del Agua, México.

Soil Survey Division Staff, 2017. Soil Survey Manual. United States Department of Agriculture, pp. 120–125. https://doi.org/10.1097/00010694-195112000-00022. Handbook No. 18.

Song, X., Ding, Y., Wang, Y., Wang, W., Wang, G., Zhou, B., 2015. Comparative study of nitrogen removal and bio-film clogging for three filter media packing strategies in vertical flow constructed wetlands. Ecol. Eng. 74, 1–7. https://doi.org/10.1016/j.ecoleng.2014.08.008.

Strakhovenko, V.D., Solotchina, E.P., Vosel, Y.S., Solotchin, P.A., 2015. Geochemical factors for endogenic mineral formation in the bottom sediments of the Tazheran lakes (Baikal area). Russ. Geol. Geophys. 10, 1437–1450. https://doi.org/10.1016/j.rgg.2015.09.006.

Stumm, W., 1992. Chemistry of the Solid-Water Interface: Processes at the Mineral-Water and Particle-Water Interface in Natural Systems. John Wiley & Sons, New York.

Sun, Y., Chen, S.S., Lau, A.Y., Tsang, D.C., Mohanty, S.K., Bhatnagar, A., Rinklebed, J., Lin, K.-Y.A., Ok, Y.S., 2020. Waste-derived compost and biochar amendments for stormwater treatment in bioretention column: co-transport of metals and colloids. J. Hazard. Mater. 383, 121243. https://doi.org/10.1016/j.jhazmat.2019.121243.

Tejeda, A., Barrera, A., Zurita, F., 2017. Adsorption capacity of a volcanic rock—used in constructed wetlands—for carbamazepine removal, and its modification with biofilm growth. Water (Switzerland) 9 (9), 721. https://doi.org/10.3390/w9090721.

Vanderzalm, J.L., Page, D.W., Barry, K.E., Dillon, P.J., 2010. A comparison of the geochemical response to different managed aquifer recharge operations for injection of urban stormwater in a carbonate aquifer. Appl. Geochem. 25 (9), 1350–1360. https://doi.org/10.1016/j.apgeochem.2010.06.005.

Walaszek, M., Del Nero, M., Bois, P., Ribstein, L., Courson, O., Wanko, A., Laurent, J., 2018. Sorption behavior of copper, lead and zinc by a constructed wetland treating urban stormwater. Appl. Geochem. 97, 167–180. https://doi.org/10.1016/j.apgeochem.2018.08.019.

Wang, S., Lin, X., Yu, H., Wang, Z., Xia, H., An, J., Fan, G., 2017. Nitrogen removal from urban stormwater runoff by stepped bioretention systems. Ecol. Eng. 106, 340–348. https://doi.org/10.1016/j.ecoleng.2017.05.055.

WHO, 2016. Barium in Drinking-Water - Background Document for Development of WHO Guidelines for Drinking-Water Quality. World Health Organization, Geneva, pp. 9–11.

Yáñez-Ocampo, G., Sánchez-Salinas, E., Jiménez-Tobon, G.A., Penninckx, M., Ortiz-Hernández, M.L., 2009. Removal of two organophosphate pesticides by a bacterial consortium immobilized in alginate or tezontle. J. Hazard. Mater. 168 (2–3), 1554–1561. https://doi.org/10.1016/j.jhazmat.2009.03.047.